Available online at **www.joac.info**

ISSN: 2278-1862

Journal of Applicable Chemistry

2019, 8 (4): 1966-1976

(International Peer Reviewed Journal)

Growth Kinetics and Thermo-Opto-Electrical Properties of Cobalt Reinforced Zinc phosphate Crystals

Delma D'Souza, N. Jagannatha* and K. P. Nagaraja

PG Department of Physics, FMKMC College, A constituent college of Mangalore University, Madikeri-571201, Karnataka State, **INDIA**

Email: jagannathnettar@yahoo.co.in

Accepted on 15th July, 2019

ABSTRACT

Cobalt doped zinc phosphate (CZP) and intrinsic zinc phosphate (IZP) crystals were grown by gel diffusion reaction technique. In the optimized growth environment with suitable Co^{2+} doping, pink coloured, hard, transparent CZP crystals were developed from the parent IZP crystals. Energy dispersive X-ray analysis (EDAX) identified Co^{2+}, Zn^{2+} and PO_4^{3-} ions complex in doped CZP crystals. FTIR spectral studies confirmed phosphate group, water molecule and M-O bond; which form armature of IZP and CZP crystals. Thermo gravimetric analysis (TGA) identified crystalline water, co-ordinated water and stability of the crystals in anhydrous phosphate phase above 500°C. P-XRD measurements depict high crystallinity of CZP and IZP crystals. IZP crystal propounded with a chemical formula $Zn_3(PO_4)_2(H_2O)_2.2H_2O$(molecular weight = 458.174) and CZP crystal manifested with a chemical formula of $(Co_{0.1228}\ Zn_{0.8772})_3(PO_4)_2H_2O.3H_2O$ (molecular weight=455.795) respectively. Optical studies unveiled insulating behaviour of parent and doped crystals. Co^{2+} cationic incorporation to Zn^{2+} vacancies increased the electrical conductivity. IZP and CZP possess dielectric constants of 18.32 and 17.53 in order. Investigation on growth aspects and thermo-opto-electrical properties merely highlighted the distinctness of CZP and IZP crystals.

Graphical Abstract

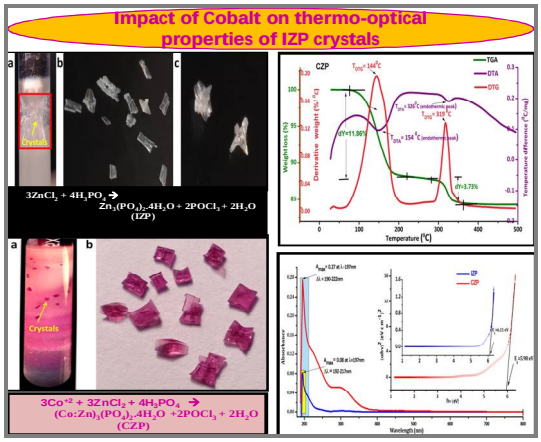

Keywords: Conductivity, Dielectric, Insulator, Silica gel, Thermal.

INTRODUCTION

In modern days, production of pure and high quality crystals is essential in the field of material science [1]. Investigation of advanced and smart materials promoted an increased demand for them in industries and laboratories [2]. Crystals grown from gels built with fine morphologies and exhibit special physical and chemical properties [3]. Barium oxalate crystals in nano scale showed semiconducting properties [4]. Studies on oxalate crystals revealed high dielectric strength in them and have wide applications [5]. Doping [9]. With careful control over the nucleation centres in gels, the resulted crystals may form new generation advanced or smart materials. Certain crystals like quartz, sodium pottassium tartrate and Polyvinylidene flouride reported peizo- electricity and also behave as smart materials [10]. GaAs, CdS and InSb crystals exhibit semiconducting properties and extensively used as infrared LEDs, solar cells and energy storage devices [11].

Earlier studies on phosphate crystals emphasized NLO properties, luminescence and corrosion resistivity [12-14]. In a refined growth environment adopting proper dopant, one can modify properties of the host crystal which propounds many new results. Only few investigations reported the doping of phosphate crystals [15, 16]. Recently we have reported the results of Cr^{3+}-Cd^{2+} matrix on oxalate crystals which emphasized the insulating behaviour, high ϵ_r and thermal stability until 950^oC in them [17]. Our present work mainly dealt on gel supported growth of phosphate crystals with Co^{2+}-Zn^{2+} matrix, their characterization and investigation on thermal, optical and electrical properties

MATERIALS AND METHODS

Single test tube gel diffusion method was employed to grow IZP and CZP crystals at ambient temperature. Chemicals used for growing IZP and CZP crystals were Sodium Meta Silicate (SMS-$Na_2SiO_3.9H_2O$), Phosphoric acid (H_3PO_4), Zinc Chloride ($ZnCl_2$) and Cobalt Chloride ($CoCl_2.6H_2O$) of AR grade.

Polymerized Silica hydro gel was prepared by mixing 1N ortho-phosphoric acid (OPA) with SMS solution. To control damage and premature gelling, OPA was added drop by drop to SMS with constant stirring. The resulted solution was transferred to different test tubes (dimension-15x125mm) 9 mL each and allowed to set for gelling [16, 18]. Gel sets in 30 hours and to the set gel the reactant mixture of 0.5M $ZnCl_2$ and 0.5M $CoCl_2$ (5:1) were added along the sides of the test tubes. Zn^{2+} ions diffused through the porous gel and nucleated with PO_4^{2-} ions. Co^{2+} ions also diffused parallelly and occupied the vacancies of Zn^{2+} ions, which resulted in the formation of doped CZP crystal. Growth process was optimized and nucleation centres were controlled by varying gel parameters and concentrations of reactant mixtures [19]. Experiment was carried out at different specific gravities of SMS (1.03-1.07 g cm^{3-1} in steps of 0.025), various concentrations of OPA (0.5-2N in steps of 0.5), concentrations of reactant solution (0.25-2M in steps of 0.25M) and ratios of Zn^{+2} to Co^{+2} in reactant mixture (ranges from 5: 0.25 to 5: 2).

Silica hydro gel of SMS specific gravity 1.045 g cm^{3-1}, Phosphoric acid of concentration 1N, in the ratio 5: 4 optimized the gel to grow good quality IZP and CZP crystals. Chemical process involved in the formation of CZP and IZP crystals are as follows.

$$3Co^{+2} + 3ZnCl_2 + 4H_3PO_4 \rightarrow (Co{:}Zn)_3(PO_4)_2.4H_2O + 2POCl_3 + 2H_2O.$$

$$3ZnCl_2 + 4H_3PO_4 \rightarrow Zn_3(PO_4)_2.4H_2O + 2POCl_3 + 2H_2O.$$

IZP and CZP crystals propounded from independent growth environment. Colour, morphology and physical appearance of intrinsic and doped crystals were different and the results were recorded in table 1. Figure 1 and 2 illuminate the growth and extraction of IZP and CZP crystals respectively.

Growth of IZP and CZP crystals in silica hydro gel spotlighted the formation of intrinsic and doped crystals with common nucleation centres, multi-nucleation and formation of liesegang rings. Initially when supernatant solution mixture ($ZnCl_2$ (0.5M) and $CoCl_2$ (0.5M) in the ratio 5:1) added over the set gel, a dense barrier below the gel interface was seen which then triggers the nucleation. As the growth advances, accumulation of charges (cations from supernatant solution mixture and anions from phosphoric acid impregnated silica gel) into the nucleation sites took place. Silica hydro gel in optimized growth environment controlled and regulated the flow of charges into nucleation sites and thereby governed the growth of IZP and CZP crystals. The charges which are restricted to flow into the nucleation sites precipitated in the form of liesegang rings [**19**].

Our investigation on growth and characterization of chromium mixed cadmium oxalate crystals [**17**] and Barium mixed oxalate crystals [**20**] in a similar growth environment have not shown the formation of liesegang rings, whereas, in the present investigation the growth of IZP and CZP crystals exhibited change in chemical process which spotlighted the crystal formation and debris into the liesegang rings. This confirms the novelty in growth environment and hence the growth of novel IZP and CZP crystals.

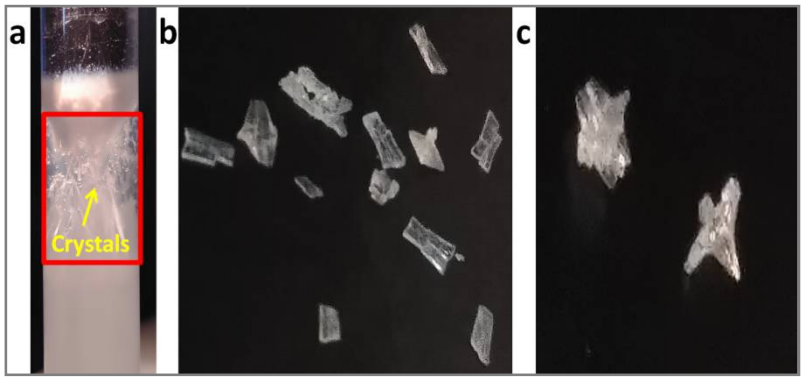

Figure 1. IZP crystals- (a) Growth in silica gel, (b) and (c) Extracted crystals.

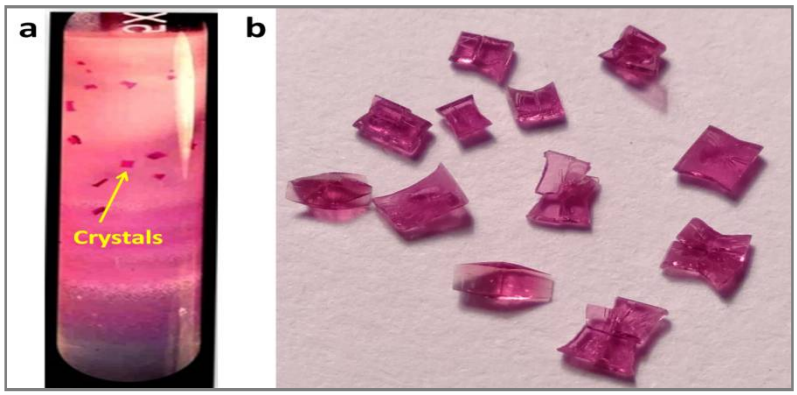

Figure 2. CZP crystals- (a) Growth in silica gel, (b) Extracted crystals.

Table 1. Optimum condition for growth.

Parameter	Crystal	
	IZP	CZP
Specific gravity	1.045	1.0375
Gel pH	6.15	5.9
SMS : H_3PO_4	5:4	5:4
Zn^{+2}: Co^{+2}	-	5 : 1
Crystal Size (l× b× h) mm^3	1.5x1.0x0.5	2.0x1.5x1.0
Colour	Colourless	Pink

Characterization: Chemical constituents of the IZP and CZP crystals were estimated using CARL ZEISS FESEM attached with EDS system (Oxford instruments) [21]. Bruker (Alpha) KBr Fourier Transform Infrared Spectrophotometer (FTIR) was used to identify the functional groups associated with the crystals. The spectrum was recorded for the wave number range 400-4500 cm^{-1} [22]. TG measurements of the grown crystals were established using DSC-TGA TA (SDT-Q600). Percentage weight loss and decomposition behaviour of IZP and CZP crystals were described for the temperature until 700°C [23]. Minflex 600 Rigaku (X-ray Cu-K alpha-wavelength 1.54A^0) at a scan speed of 1˚ $minute^{-1}$ was used to study the X-Ray Diffraction patterns of powdered crystalline samples of IZP and CZP crystals. Impact of UV-visible light on intrinsic and doped crystals were analyzed with the aid of UV-Visible spectrophotometer (UV-1800 Schimadzu) in the spectral range 200-1200 nm. Electrical conductivity measurements of the crystals were recorded using Roy instruments (IR-503, S. No. CDM-17076) operated for the conductivity range 0-1000 mMho/cm [17]. Dielectric studies were performed using Mittal instruments 2151/T-7C calibrated for sine wave of frequency 253.88 kHz in DSO.

RESULTS AND DISCUSSION

Chemical composition of IZP and CZP crystals were determined using EDX spectra. In FESEM arrangements powdered crystalline samples (IZP and CZP) were subjected to electron bombardment, which radiated the X-Rays. The plot of X-Ray energies released, extinguished as intense peaks which illuminate the characteristics of the elements Zn, Co, O and P present in the crystals. The resulted characteristic peaks and representative elements existing in IZP and CZP crystals are clearly seen in EDX spectra (Figure 3). Composition of elements present in the crystals is recorded in the table 2. FESEM images of IZP and CZP are displayed in Figure 4. At the resolution 100x with separation 100 µm from the sample crystal, both the crystals exhibited best morphology and very rare surface damages.

The EDX measurements of IZP and CZP crystals confirmed Co^{2+} ions doping which merely occupied the Zn^{2+} vacancies. The estimated Zn^{2+}: Co^{2+} cationic distribution is 7.15:1. Co^{2+} ions can fit well in Zn^{2+} vacancies due to similar ionic radii (Zn^{2+}-0.88A°, Co^{2+}-0.89A°) and comparable electro-negativities (Zn-1.66, Co -1.70). According to EPR studies on Zn^{2+}-Co^{2+} matrix; the co-ordination geometry of Zn^{2+} and Co^{2+} cations are similar (octahedral). The difference in chemical constituents, dissimilarities in morphologies confirmed Co^{2+} ion doping in the formation of novel CZP crystal.

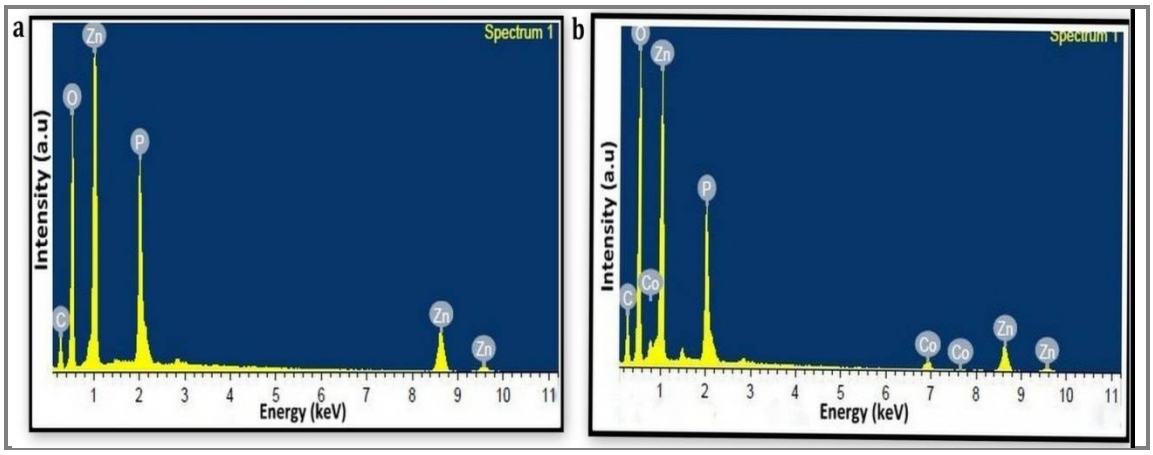

Figure 3. EDX spectra of IZP (a) and CZP (b) crystal.

FTIR spectra of IZP and CZP crystals exhibited number of absorption bands correspond to various functional groups (Figure 5). Both the crystals show similar spectra but exhibit shift in absorption bands.

Table 2. Chemical constituents of IZP and CZP crystals

Crystal	Elements Present	Weight %	Atomic %
IZP	Zn	43.790	18.220
	P	16.770	14.731
	O	39.440	67.049
CZP	Zn	36.970	14.370
	Co	04.670	02.010
	O	46.550	73.930
	P	11.810	09.690

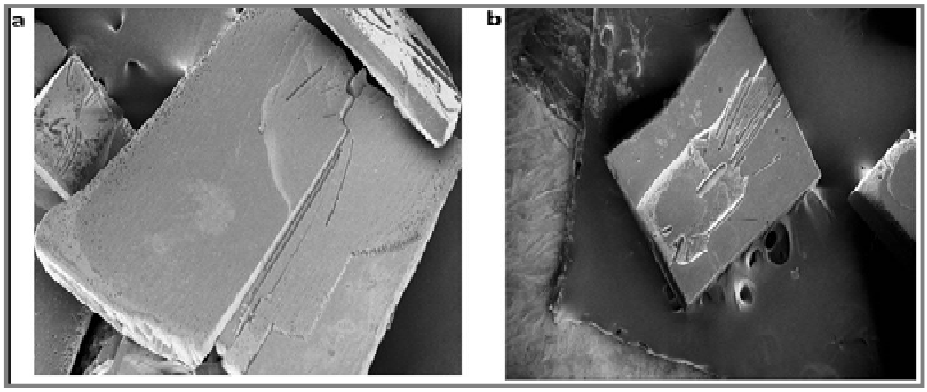

Figure 4. FESEM images of (a) IZP and (b) CZP crystals.

Spectra identified water molecules, PO_4 units, metal oxygen bonds (M–O) and transition metals (Zn and Co) as constituents of parental and doped crystals. Absorption in the range 3762 cm^{-1} to 3169 cm^{-1} attributed to symmetric and asymmetric stretching of O-H group, indicates water of crystallization. Bending vibration of water molecules exists at 1603 cm^{-1} for both parental and doped crystals [23]. The absorption band around 1400 cm^{-1} corresponds to P=O stretching [24]. The spectra record asymmetric stretching of P-O bond around 1107 cm^{-1} for IZP crystal, where as for CZP crystal this resulted at 1023 cm^{-1}. The peak at 948 cm^{-1} was due to P-O symmetric stretching. In the finger print region both the crystals exhibited O-P-O asymmetric bending around 635cm^{-1} and 578 cm^{-1} respectively. The vibrations in the range 414-430 cm^{-1} represent O-P-O symmetric bending [25]. The dissimilarities in fingerprint region of CZP and IZP crystals confirm the matrix of Co^{2+}-Zn^{2+} in doped crystal. Table 3 outlines the band assignments for absorption peaks of IZP and CZP crystals.

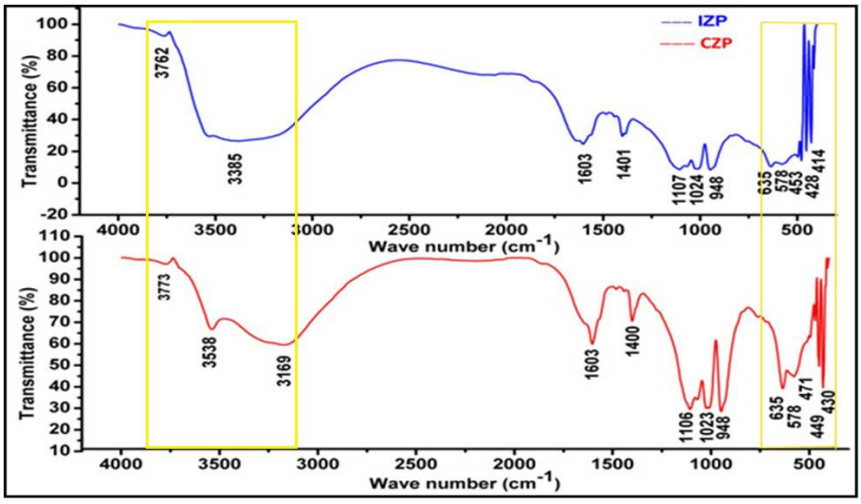

Figure 5. FTIR spectra of IZP and CZP crystals.

Table 3. FTIR results of IZP and CZP crystals

Band assignments	Wave number (cm^{-1})	
	IZP	CZP
Symmetric and asymmetric O-H stretching (water of Crystallization)	3762 3385	3773 3538 3169
Internal bending vibration of water molecule s	1603	1603
P=O stretching	1401	1400
Asymmetric P-O stretching	1107 1024	1106 1023
Symmetric P-O stretching	948	948
Asymmetric O-P-O bending	635 578	635 578
Symmetric O-P-O bending	428	430

Thermal stability and decomposition status of IZP and CZP crystals were analysed using TG plots (Figure 6 and Figure 7). TG analysis of IZP and CZP showed association of four water molecules in both IZP and CZP crystals. However, the decomposition behaviour of the parent and doped crystals were different.

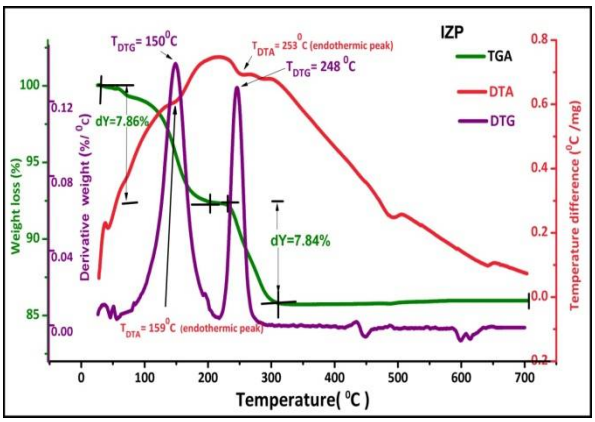

Figure 6. TG plot of IZP crystal

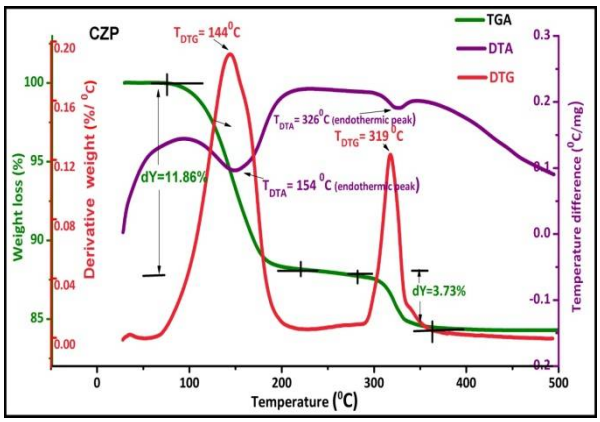

Figure 7. TG plot of CZP crystal.

TG results of IZP and CZP crystals were shown in table 4 and table 5. First phase of decomposition in IZP crystal occurred in the temperature range 37-195°C with observed weight loss of 7.86% (Calculated loss: 7.864%) at the loss of two crystalline water. T_{DTG} peak for this structural deformation occurs at 150°C and corresponding T_{DTA} endothermic peak at 159°C. Second phase of decomposition accomplished in the T_d range 240-315°C with T_{DTG} peak at 248°C and endothermic T_{DTA} peak at 253°C suffering a weight loss (observed) of 7.84% (Calculated loss: 7.864%) losing a matter of two co-ordinated water molecules and remains stable in anhydrous state.

Figure 7 illuminates the TG plot of CZP crystal. Incorporation of Co^{2+} cationic complex in ZP crystal altered the structural deformation of CZP crystal in its two phases. In the first phase of degradation (T_D range 92 -223°C) CZP crystal loses three molecules of crystalline water suffering a weight loss (observed) of 11.86% (Calculated loss: 11.857%). In the second decomposition phase (T_D 295-360°C) CZP crystal lost one co-ordinated water molecule with observed weight loss of 3.73% (Calculated loss: 3.952%). Above 360°C, crystal exists in the anhydrous state until 500°C. DTG and DTA peaks corresponding to first decomposition phase occurs at T_{DTG}=144°C and T_{DTA}=154°C respectively. Further, in second degradation phase peaks fall at T_{DTG}=319°C and T_{DTA} = 326°C.

The TG studies with evaluation by EDAX and FTIR characterization unveiled the chemical formula of IZP crystal as $Zn_3(PO_4)_2(H_2O)_2.2H_2O$ extinguishing a molecular weight of 458.74. Additionally, novel CZP crystal come out with a chemical formula $(Co_{0.1228}Zn_{0.8772})_3(PO_4)_2H_2O.3H_2O$ possessing a molecular weight of 455.795.

TG regime of IZP crystals confirms the existence of two crystalline water and two co-ordinated water bound to the crystal, whereas, in CZP crystals TG profile shows the presence of three crystalline water and one co-ordinated water. The variation in the results is mainly due to modulation in co-ordination environment of parental crystal imposed by Co^{2+} ion. According to EPR studies [**26**] on Co^{2+}-Zn^{2+} complex, site symmetry of Zn^{2+} ions is similar to that of Co^{2+} ions and doping ions can fit well in the vacancies of Zn^{2+} ions. In addition to this, in our investigation, TG studies followed by EDAX and FTIR analysis evidence the Co^{2+} doping into Zn^{2+} vacancies and come out with a cationic distribution of 7.15:1(Zn^{2+} : Co^{2+}) which reflects the success of developing novel CZP crystal.

Table 4. Decomposition behaviour of IZP and CZP crystals

Crystal	Phase	Decomposition Temp T_D(°C)	Weight loss (%)		Decomposition Process
			Observed	Calculated	
IZP	I	37-195	07.86	07.864	$Zn_3(PO_4)_2(H_2O)_2.2H_2O \rightarrow Zn_3(PO_4)_2(H_2O)_2 + 2H_2O$
	II	240-315	07.84	07.864	$Zn_3(PO_4)_2(H_2O)_2 \rightarrow Zn_3(PO_4)_2 + 2H_2O$
CZP	I	92-223	11.86	11.857	$(Co:Zn)_3(PO_4)_2H_2O.3H_2O \rightarrow (Co:Zn)_3(PO_4)_2H_2O + 3H_2O$
	II	295-360	03.73	03.952	$(Co:Zn)_3(PO_4)_2H_2O \rightarrow (Co:Zn)_3(PO_4)_2 + H_2O$

Table 5. TG results of IZP and CZP crystals

Crystal	Chemical formula	Molecular weight	Phase	T_{DTG} (°C)	T_{DTA} (°C)	Molecule decomposed
IZP	$Zn_3(PO_4)_2(H_2O)_2.2H_2O$	458.74	I	150	159	$2H_2O$
			II	248	253	$2H_2O$
CZP	$(Co_{0.1228}Zn_{0.8772})_3(PO_4)_2H_2O.3H_2O$	455.795	I	144	154	$3H_2O$
			II	319	326	H_2O

Powder XRD Bragg's reflections of IZP and CZP crystals were recorded for different 2θ values in the range from 8-90°. Figure 8 and figure 9 illuminate the Bragg X-Ray diffraction patterns of parental and doped crystals respectively. High intensity peaks of CZP crystal elucidate superior crystallinity than IZP crystal. N-TREOR09 program was used to index the peaks of P-XRD plots. Results obtained are in agreement with the standard values of JCPDS data reported [**25**]. Both IZP and CZP crystals exists in orthorhombic system. The lattice parameters of IZP and CZP crystals were recorded in Table 6.

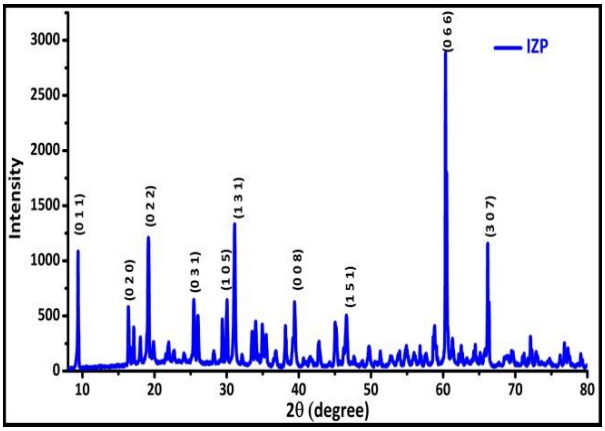

Figure 8. Powder XRD pattern of IZP crystal.

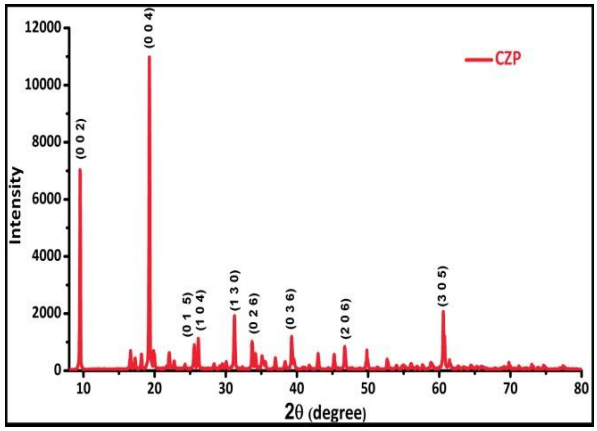

Figure 9. Powder XRD pattern of CZP crystal.

Table 6. Lattice parameters of IZP and CZP crystals

Lattice parameters	IZP	CZP
a (A^0)	05.0275	05.05
b (A^0)	10.6007	10.51
c (A^0)	18.2630	18.24
α (^{0})	90	90
β (^{0})	90	90
γ (^{0})	90	90
Space group	*Pbnm*	*Pbnm*
System	Orthorhombic	Orthorhombic

Optical properties using UV-visible spectroscopy exhibits the extent of transparency of the crystals to the UV-Visible light [27]. Figure 10 (a**)** shows the UV-Visible absorbance spectra of IZP and CZP crystals. In the entire visible region both crystals showed maximum transparency. Tauc plots (Figure 10 (b)) were developed to determine band gap energies of parental and doped crystals. Resulted band gap energies of IZP and CZP crystals are 6.11eV and 5.98eV respectively and crystals behave as insulators. Further, IZP crystal showed selective absorption in the wavelength range 19-217 nm (correspond to UV region) with absorption maximum (A_{max}) of 0.08 at the resonant wavelength 197 nm. Absorption (A) decays exponentially, from 218 nm till 800 nm (IR). However, CZP crystal showed selective absorption for the absorption band extended from 191nm to 222 nm with A_{max} 0.27. Above 232 nm, absorption follows exponential decay in two steps (I step: 232- 302 nm and II step: 303-400 nm) due to impact of Co^{2+} doping. Co^{2+} incorporation to IZP crystal widens the absorption band, increases sharpness of resonance but retains the resonant wavelength (197 nm).

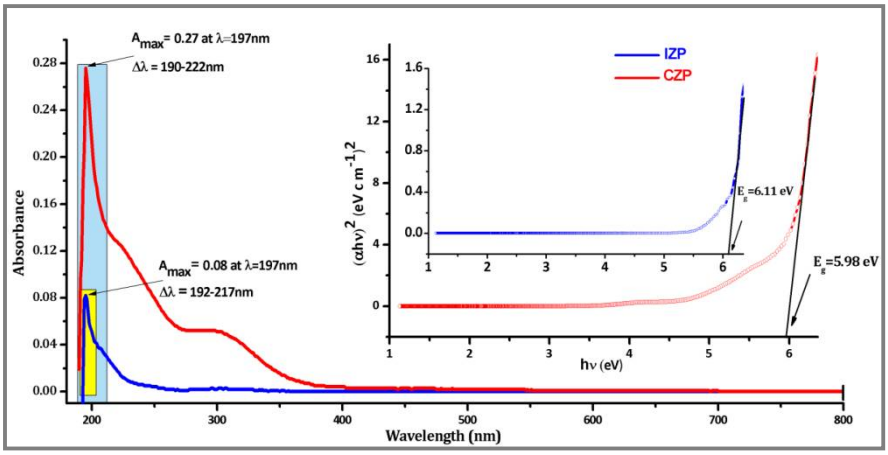

Figure 10. UV-visible absorbance spectrum (a) and tauc plots (b) of IZP and CZP crystals.

Electrical conductivity measurements of IZP and CZP crystals were carried out by dissolving 10 mg of crystals in 100 mL of H_2SO_4 (1.5N) at ambient temperature [28]. In view of heating effects of solids, electrical conductivities of the crystals were measured at two distinct temperatures, viz., 27^{0}C (room temperature) and 40°C (working temperature of electrical circuits). After calibration, the measured electrical conductivities of IZP and CZP crystals are recorded in table 7. Conductivity measurements showed improvement in conductivity due to Co^{2+} doping on parental crystal and suggest that the crystals are better dielectrics at ambient temperature.

Table 7. Electrical conductivities of IZP and CZP crystals.

Crystal	Electrical conductivity mʊ/cm	
	27^{0}C	40^{0}C
IZP	0.5	0.3
CZP	4.6	2.7

Dielectric measurements of IZP and CZP crystals were conducted for pelletized crystals of thickness approximately 1*mm* and area equal to the dimension of gold plated dielectric cell [**20**].Using dielectric constant measuring unit, the capacitance (C) of IZP and CZP crystals measured as

$$C = \frac{V_{sc} C_S}{V_{dc}}$$

Where, V_{sc} is the dc voltage across standard capacitance C_s and V_{dc} is the dc voltage measured across test crystals. Capacitance C_o of air measured as

$$C_o = \frac{\epsilon_0 A}{d}$$

Where, ε_o is absolute permittivity of free space, A and d are cross-sectional area and thickness of crystal pellets respectively. Dielectric constant ε_r of the crystals measured as

$$\epsilon_r = \frac{C}{C_o}$$

Table 8. Dielectric properties of IZP and CZP crystals

Crystal	C (pF)	ε_r
IZP	31.922	18.32
CZP	30.545	17.53

APPLICATION

Investigation on thermal properties, UV-visible spectroscopic studies, electrical conductivity and dielectric measurements revealed that IZP and CZP crystals are thermally stable in anhydrous state above 500°C and exhibited insulating behaviour with high band gap energies. Co^{2+} doping in CZP crystal enhanced its conductivity and the crystal is suitable to use as dielectric at ambient temperature. The insulating behaviour, extended dielectric strength and good thermal stability possessed by the crystals gather a spectrum of microelectronic and optoelectronic applications. Hence investigation on opto-electrical properties of the IZP and CZP crystals provides wide scope for research and with concentrated work, above crystals possibly come out as new smart material.

CONCLUSION

IZP and CZP crystals were successfully grown adopting gel method in independent growth environments spotlighted the debris in liesegang rings. EDAX measurements confirmed the existence of Co^{2+} and Zn^{2+} ions in the doped CZP crystal. FTIR results and TG plots of the parental and doped crystals elucidated the structural units, decomposition behaviour and established chemical formulae as $Zn_3(PO_4)_2(H_2O)_2.2H_2O$ for IZP crystal and $(Co_{0.1228}Zn_{0.8772})_3(PO_4)_2H_2O.3H_2O$ for CZP crystal respectively. PXRD studies predicted high crystalline nature of the crystals and their existence in orthorhombic system. UV-visible spectral studies measured the band gap energies and with the evidence of electrical conductivity measurements both IZP and CZP crystals behave as insulators. Investigation on growth, characterization and properties of IZP and CZP crystals emphasized that the crystals as cluster and coordination geometry of crystalline water, co-ordinated water, induced Co^{2+}-Zn^{2+} matrix and inorganic PO_4 units, which in turn highlighted the success in the formation of novel IZP and CZP crystals.

ACKNOWLEDGEMENTS

The authors are thankful to UGC New Delhi for financial support under the MANF scheme and grateful to scientific officer, DST- PURSE laboratory, Mangalore University, Mangalore for providing laboratory facilities.

REFERENCES

[1]. Hongwei Huang, Chuangtian Chen, Xiaoyang Wang, Yong Zhu, Guiling Wang, Xin Zhang, Lirong Wang, Jiyong Yao, Ultraviolet nonlinear optical crystal: $CsBe_2BO_3F_2$, *J. Opt. Soc. Am. B.*, **2011**, 28(9), 2186-2190.
[2]. Abeer Samy Yousef Mohamed, Smart materials innovative technologies in architecture; towards innovative design paradigm, *Energy Procedia*, **2017**, 115, 139-154.
[3]. V. Mathivanan, M. Harish, Structural, compositional, optical, thermal and magnetic analysis of undoped, copper and iron doped potassium hydrogen tartrate crystals, *Indian J. of Pure and Applied Phys.*, **2013**, 51, 851-859.
[4]. S. K. Arora, V. Patel, B. Chudasama, B. Amin, Single crystal growth and characterization of strontium tartrate, *J. Cryst. Growth*, **2005**, 275, e657-661.
[5]. K. P. Nagaraja, K. J. Pampa, N. K. Lokanath, Studies on Growth, optical, electrical and dielectric properties of strontium and calcium mixed cadmium oxalate crystals, *J. Applicable. Chem.*, **2018**, 7, 457-66.
[6]. K. Rajendran , C. Dale Keefe, Growth and characterization of calcium hydrogen phosphate dihydrate crystals from single diffusion gel technique, *Cryst. Res. Technol.*, **2010**, 45, 939-945.
[7]. V. Mahalakshmi, A. Lincy , J. Thomas, K.V. Saban, Crystal growth and characterization of a new co-ordination complex – barium tetrakis(maleate) dihydrate, *J. Phy. Chem. Sol.* , **2012**, 73, 584-588.
[8]. P. P. Pradyumnan, C. Shini, Growth characterization and etching studies of calcium tartrate single crystal grown using tamarind extract, *Ind. J. Pure Appl. Phys.*, **2009**, 47, 199-205.
[9]. N. Jagannatha, P. Mohan Rao, Studies on impurity incorporation in cadmium oxalate crystals grown by gel method. *Bull. Mater. Sci.*, **1993**, 16, 365-370.
[10]. D. Wang, J. S. Chen, Progress on the applications of piezoelectric materials in sensors. *Mater. Sci. Forum*, **2016**, 848, 749-756.
[11]. Xiangfeng Duan, Charles M. Lieber, General synthesis of compound semiconductor nanowires, *Adv. Mater.*, **2000**, 12, 298-302.
[12]. H. Onoda, H. Nariai, H. Maki, I. Motooka, Mechanochemical effects of some rare-earth ultraphosphate and reforming of their surface for catalytic properties, *Phosphorus Res. Bull.* **1999**, 9, 69-74.
[13]. S. Haussu¨hl, B. Middendorf, M. Do¨rffel, Structure and properties of hopeites $(Mg_xZn_{1-x})_3(PO_4)_2{\cdot}4H_2O$. *J. Sol. State Chem.* **1991**, 93, 9-16.
[14]. Xiao-Bo Chen, Xian Zhou, B.A. Trevor, A.E. Mark, Nick Birbilis, Double-layered manganese phosphate conversion coating on magnesium alloy AZ91D: Insights into coating formation, growth and corrosion resistance, *Surface and Coatings Technology*, **2013**, 217, 147-155.
[15]. K. K. Bamzai, Shivani Suri, Vishal Singh, Synthesis, characterization, thermal and dielectricproperties of pure and cadmium doped calcium hydrogen phosphate, *Mater. Chem. Phys.*, **2012**, 135, 158-167.
[16]. M. S. Valsamma, N. V. Unnikrishnan, M. A. Ittyachen, Thermal characteristics of pure and neodymium doped calcium hydrogen phosphate single crystals, *J. Therm. Anal. Calorim.*, **2009**, 96:917-921
[17]. Nagaraja Ponnappa, Jagannatha Nettar, Hema Mylnahalli, Delma D'Souza, Lokanath Neratur, Growth, characterization and conductivity of chromium mixed cadmium oxalate crystals, *Cryst. Res. Technol.*, **2018**, 53, 1700261.
[18]. D. Nallamuthu, Selvarajan, T. H. Freeda. Studies on various properties of pure and Li-doped barium hydrogen phosphate (BHP) single crystals, *Physica B* **2010**, 405, 4908-4913.

[19]. S. M. Dharmaprakash, P. Mohan Rao, Periodic crystallization of barium oxalate in silica hydrogel. *Bull. Mater. Sci.,* **1986**, 8, 511-517.
[20]. K. P. Nagaraja, Delma D'Souza, K. J. Pampa, N. K. Lokanath, Impact of barium cationic mixing on cadmium and strontium oxalate crystals, *Mater. Res. Express,* **2019**, 6, 035506.
[21]. J. G. Yu, H.Tang, B. Cheng, Influence of PSSS additive and temperature on morphology and phase structures of calcium oxalate, *J. Colloid and Interface Sci.,* **2005**, 288, 407-411.
[22]. E. D. Bacce, A. M. Pires, M. R Davaios, M. Jafelicci Jr, Thermal decomposition and rehydration of strontium oxalate: q morphological evolution, *International J. of Inorganic Mate,*. **2001**, 3, 443-452.
[23]. S. Vimal Joshi , J . Mihir Joshi, FTIR spectroscopic, thermal and growth morphological studies of calcium hydrogen phosphate dihydrate crystals, *Cryst. Res. Technol.*, **2003**, 38, 817-821.
[24]. C. Justin Raj, G. Mangalam, S. Mary Navis Priya , J. Mary Linet, C. Vesta, S. Dinakaran, B. Milton Boaz, S. Jerome Das, Growth and characterization of nonlinear optical zinc hydrogen phosphate single crystal grown in silica gel, *Cryst. Res. Technol.*, **2007**, 42, 344-348.
[25]. Laurent Herschke, Volker Enkelmann, Ingo Lieberwirth, Gerhard Wegner, The role of hydrogen bonding in the crystal structures of zinc phosphate hydrates, *Chem. Eur. J.*, **2004**,10, 2795-803.
[26]. B. Bennett, EPR of cobalt-substituted Zinc enzymes. In: Hanson G., Berlier L. (eds) Metals in Biology. Biological Magnetic resonance, 29, Springer, New York, NY.
[27]. P. Anandan , G. Parthipan, T. Saravanan, R. Mohan Kumar, G. Bhagavannarayana, Jayavel R. Crystal growth, structural and optical characterization of a semi-organic single crystal for frequency conversion applications, *Physica B*, **2010**, 405, 4951-4956.
[28]. T. H. Freeda, C. Mahadevan, Electrical conductivity measurements on gel grown KDP crystals added with some ammonium compounds, *Bull. Mater. Sci,*. **2000**, 23, 335-340.